A Meshfree procedure for the microscopic analysis of particle-reinforced rubber compounds

C. T. Wu[†]

Livermore Software Technology Corporation, Livermore, CA 94550, USA

M. Koishi[‡]

CAE Laboratory, The Yokohama Rubber Co, Ltd., Japan

Abstract. This paper presents a meshfree procedure using a convex generalized meshfree (GMF) approximation for the large deformation analysis of particle-reinforced rubber compounds on microscopic level. The convex GMF approximation possesses the weak-Kronecker-delta property that guarantees the continuity of displacement across the material interface in the rubber compounds. The convex approximation also ensures the positive mass in the discrete system and is less sensitive to the meshfree nodal support size and integration order effects. In this study, the convex approximation is generated in the GMF method by choosing the positive and monotonic increasing basis function. In order to impose the periodic boundary condition in the unit cell method for the microscopic analysis, a singular kernel is introduced on the periodic boundary nodes in the construction of GMF approximation. The periodic boundary condition is solved by the transformation method in both explicit and implicit analyses. To simulate the interface de-bonding phenomena in the rubber compound, the cohesive interface element method is employed in corporation with meshfree method in this study. Several numerical examples are presented to demonstrate the effectiveness of the proposed numerical procedure in the large deformation analysis.

Keywords: meshfree; microscopic; periodic boundary condition; basis function; Kronecker-delta property; unit cell

1. Introduction

   Meshfree methods are the topic of recent research in many areas of computational science and engineering. One of the early incentives to develop meshfree method was its ability to handle large deformation problems (Chen *et al.* 1996). Other advantages of the meshfree methods can also be found in many literatures (Belytschko *et al.* 1996, Li *et al.* 2002). In general, meshfree shape functions can be categorized into two groups, the approximation methods and the interpolation methods. There are two well-known approximation methods, the moving least-squares (MLS) approximation (Lancaster and Salkauskas 1981, Belytschko *et al.* 1994) and the reproducing kernel

---

[†] Senior engineer, Email: ctwu@lstc.com
[‡] General manager, Email: koishi@hpt.yrc.co.jp

(RK) approximation (Liu *et al.* 1995, Chen *et al.* 1996). The MLS approximation was achieved by solving a linear constrained quadratic minimization problem and the RK approximation was achieved by introducing a correction function to the smooth particle hydrodynamics (SPH) approximation (Lucy 1977) to guarantee the reproducing condition. It was shown that MLS and RK approximations are actually same methods but derived in a different way (Belytschko *et al.* 1996). Meshfree approximation methods do not satisfy the Kronecker-delta property at the boundary, which is an important property to impose the essential boundary conditions. In order to impose the essential boundary conditions, there are several special treatments have been proposed, such as Lagrange multiplier method (Belytschko *et al.* 1994), transformation method (Chen *et al.* 1996), mixed transformation method and singular kernel method (Chen and Wang 2000), coupling with finite element method (FEM) (Belytschko *et al.* 1995, Rabczuk *et al.* 2006), and so on.

A well-known interpolation method is the radial basis functions (RBF), which are invariant under all Euclidean transformations. The classic form of RBF is the multiquadrics (MQ) (Kansa 1992a, 1992b). There are other forms of RBF, such as thin plate spline (TPS) (Duchon 1976) and Gaussian radial function (Powell 1992). The major advantage of these methods is the satisfaction of the Kronecker-delta condition. However, they are limited to small-scale problems because of their nonlocality. Some expanded and combined methods were proposed to overcome the limitations, such as non-Sibsonian interpolation (Belikov and Semenov 2000), point interpolation method (PIM) (Liu and Gu 2001), moving kriging (MK) interpolation method (Gu 2003), weighted radial basis collocation method (Hu *et al.* 2007), and more recently the combined RK and RBF approximation (Chen *et al.* 2008).

On the other hand, a novel approximation scheme was also introduced recently, the so-called maximum entropy (ME) approximation (Sukumar *et al.* 2004, Arroyo and Ortiz 2006). The ME approximation is developed based on the Shannon's entropy concept (Shannon 1948) and ME principle (Jaynes 1957), which is a convex approximation and satisfies Kronecker-delta property at the boundary. Also, this approximation guarantees the unique solution inside a convex hull with a minimum distributed data set. More recently Wu *et al.* (2009) further extended the ME approximation to a generalized approximation and called it a "generalized meshfree (GMF) approximation". The method can be used to construct various convex and non-convex meshfree approximations with the ease of essential boundary condition treatments.

Applications of meshfree method in multi-scale constitutive modeling of heterogeneous materials are still somewhat rare. An interface-enriched reproducing kernel approximation was introduced by Wang *et al.* (2003) for the homogenization of magnetostrictive particle-filled elastomers. Terada *et al.* (2003) proposed a finite cover method which is an Eulerian type of meshfree method for the large deformation analysis of composite materials. Chen *et al.* presented two multi-scale wavelet methods on the analysis of heterogeneous materials with fixed and evolving microstructures (Chen and Mehraeen 2004, 2005).

In this study, we first investigate the Kronecker-delta property in GMF approximations for the microscopic analysis of rubber compounds. The choose of positive and monotonic increasing basis function in GMF approximation leads to a convex meshfree approximation that guarantees the continuity of approximation across the material interface in the rubber compounds. In order to impose the periodic boundary condition in the unit cell, a singular kernel is introduced in corporation with the GMF basis function to acquire the "strong" Kronecker-delta property on the periodic boundary. To solve the periodic boundary condition numerically, a transformation method based on the multiple constraints concept is employed. The computational formulation is formed in the framework of Galerkin meshfree method based on a GMF approximation. The final discrete equations are condensed and solved for the retained nodes. The dependent nodes are obtained from

the constraint equations. Both implicit and explicit formulations are presented. In order to consider the de-bonding phenomena in the microscopic analysis of rubber compound, the cohesive interface element formation is derived in conjunction with explicit meshfree formulation. Using the proposed approach, we analyzed three large deformation problems on microscopic level including the de-bonding of material interface.

This paper is organized as follows: The GMF approximation is reviewed and the Kronecker-delta property of GMF approximation is discussed in section 2. In section 3, the transformation method is employed to solve the periodic boundary condition in meshfree method. Section 4 presents the implicit and explicit meshfree formulations for the periodic boundary value problem. In addition, the cohesive interface element formulation is derived for the be-bonding analysis. Several numerical examples are presented in section 5 to demonstrate the effectiveness of the approach, followed by conclusions and discussions in section 6.

2. Review of Generalized meshfree (GMF) approximation

In the Maximum Entropy approximation, the basis function considers the exponential distribution of the probability. Therefore it implies that the approximation is convex since the exponential function is non-negative. It is noted that other members in the exponential family of probability density function also can be chosen as a basis function and different entropy measure also can be used to obtain the convex approximation. Motivated by the ME theory, the choice of different basis function can now be considered as the choice of different "weighted" distribution which may not necessarily be a convex function and members of the exponential family. Moreover, it is possible that the basis function also can be translated and blended with other functions to generate a particular approximation locally or globally while still keeping the smoothness and reproducing conditions. The construction of generalized meshfree approximation can be viewed as a root-finding scheme of linear reproducing functions that enforces the basis functions to be corrected and the linear reproducing conditions to be satisfied within a set of nodes.

2.1. GMF approximation

The GMF approximation (Wu *et al.* 2009) in one dimension is introduced in following form:

$$\Psi_i(\mathrm{x}, \lambda_1) = \frac{\psi_i}{\psi} = \frac{\phi_a(\mathrm{x}; X_i)\Gamma_i(X_i, \lambda_1)B(X_i, \lambda_1, \Theta)}{\Sigma_{j=1}^n \phi_a(\mathrm{x}; X_j)\Gamma_j(X_j, \lambda_1)B(X_j, \lambda_1, \Theta)} \quad \text{for fixed x} \tag{1}$$

subject to
$$R_1(\mathrm{x}) = \sum_{i=1}^n \psi_i X_i = 0 \quad \text{(linear constraints)} \tag{2}$$

where
$$\psi_i = \phi_a(\mathrm{x}; X_i)\Gamma_i(X_i, \lambda_1)B(X_i, \lambda_1, \Theta) \tag{3}$$

$$\psi = \Sigma_{i=1}^n \psi_1 = \Sigma_{i=1}^n \phi_a(\mathrm{x}; X_i)\Gamma_i(X_i, \lambda_1)B(X_i, \lambda_1, \Theta) \tag{4}$$

$$X_i = \mathrm{x} - \mathrm{x}_i \tag{5}$$

$\phi_a(\mathrm{x}; X_i)$ is the weighting function of node *i* with support size *a* (x),

$\Gamma_i(X_i, \lambda_1)$ is the basis function,

x is the coordinate of interior point (fixed point),

x_i is the coordinate of node i,

n is the number of nodes with their support cover x,

$\lambda_1(x)$ is the constraint parameter which has to be decided,

$B(X_i, \lambda_1, \Theta)$ is the blending function and Θ is internal functions or variables.

In the GMF approximation, the property of the partition of unity is automatically imposed by Eq. (1). The completion of the GMF approximation is achieved by finding $\lambda_1(x)$ to satisfy Eq. (2). To determine $\lambda_1(x)$, a root-finding algorithm such as Newton's method is required.

It was shown by Wu *et al.* (2009) that GMF approximation could be degenerated to several well-known meshfree approximations if an appropriate basis function is chosen in Eq. (3). For example, when the basis function is chosen to be the exponential function, the GMF approximation is degenerated to the ME approximation. MLS and RK approximations can also be restored if polynomial function is adopted as the basis function in GMF approximation. The smoothness of the basis function controls the smoothness of the resulting GMF approximation. It was shown that the convex approximation is obtained if a positive basis function such as exponential function is used in the construction of GMF approximation. The positive approximation ensures the positive mass in the discrete system. It is also recognized that the positivity of the approximation minimizes the effects of support size and integration order in meshfree method (Wu *et al.* 2009).

The weighting function in Eq. (1) plays similar role as in the MLS and RK approximations which introduces the local approximation as well as contributes to the smoothness of the GMF approximation. The weighting function is a translation and scaling of a compactly supported kernel function. In this paper, we choose the cubic spline function as the kernel function.

The blending function in Eq. (1) is introduced to modify the basis function for the generation of a particular GMF approximation with special purpose. For example, it was shown (Wu *et al.* 2009) that by incorporating a positive blending function with any non-positive basis function on the boundary, the weak Kronecker-delta property for the non-convex approximation such as MLS could be achieved. Other applications of the blending function include the imposition of second-order approximation and the translation of basis function to control the convex and non-convex properties of the approximation.

2.2. Kronecker-delta property of GMF approximation

This section investigates the Kronecker-delta property of GMF approximation in order to impose the periodic boundary conditions as well as to guarantee the continuity of approximation across the interface in the meshfree analysis of rubber compounds on the microscopic level. In GMF approximation, shape functions constructed using non-positive basis functions such as polynomial functions do not pose the Kronecker-delta property at the boundary unless a blending function or special boundary condition treatments are introduced (Wu *et al.* 2009). In contrast, a weak Kronecker-delta property is automatic satisfied in a convex GMF approximation when a positive basis function is adopted, i.e.

$$\mathbf{conv}(C) = \left\{ \sum_{i=1}^{nb} \Psi_i \, x_i \middle| x_i \in C, \Psi_i \geq 0, \sum_{i=1}^{nb} \Psi_i = 1 \right\} \tag{6}$$
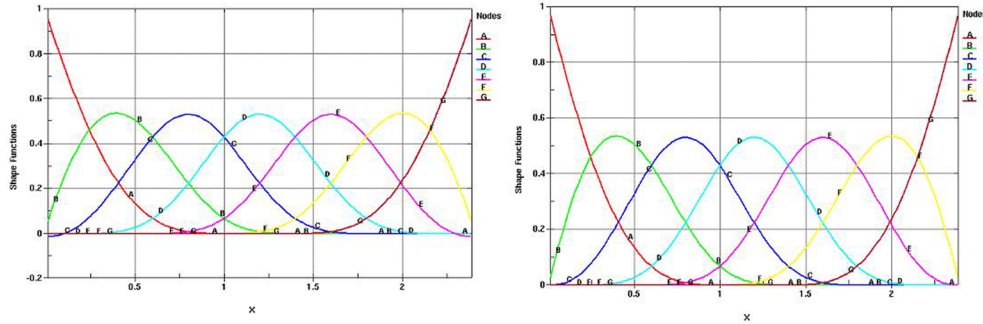
Fig. 1 Shape functions of GMF approximation function: (a) non-convex approximation (b) convex approximation

where *nb* is the number of boundary nodes. In general, the boundary nodes in the convex approximation still satisfy the Kronecker-delta property $\Psi_i(\mathrm{x}_j) = \delta_{ij}$ even in the multi-dimensional case. But for the nodes that are collinear in two-dimension or coplanar in three-dimension on the boundary of the domain, the Kronecker-delta property does not hold. However, the shape functions of interior nodes in the convex approximation still do not contribute to the boundary nodes as in the Kronecker-delta property case and the partition of unity property of the boundary nodes still pose.

Fig. 1(a) shows the one-dimension GMF shape functions using the polynomial basis function which do not have the weak Kronecker-delta property on the boundary. In contrast, Fig. 1(b) shows the one-dimension GMF shape functions using the exponential basis function possess the weak Kronecker-delta property on the boundary. Noted that the shape functions inside the domain do not have Kronecker-delta property. Convex GMF approximation can also be generated by other positive basis functions which are given by

(i) Hyperbolic tangent function: $tanh(x) + 1$

(ii) Inverse tangent function: $\dfrac{2}{\pi} tan^{-1}(x) + 1$

(iii) Hyperbolic secant function: $\begin{cases} sech(x) & (x < 0) \\ 2 - sech(x) & (x \geq 0) \end{cases}$

(iv) Radial basis function (RBF): $\begin{cases} \dfrac{1}{\sqrt{x^2 + c^2}} & (x < 0) \\ 2 - \dfrac{1}{\sqrt{x^2 + c^2}} & (x \geq 0) \end{cases}$ (*c*: shape parameter)

(v) Combination of the above functions or other positive functions

To impose the Kronecker-delta property for any interior node, one can incorporate a singular kernel in the blending function Eq. (3) as introduced in the conventional meshfree methods (Chen and Wang 2000). Fig. 2 shows the singularity is introduced in the one-dimension GMF shape
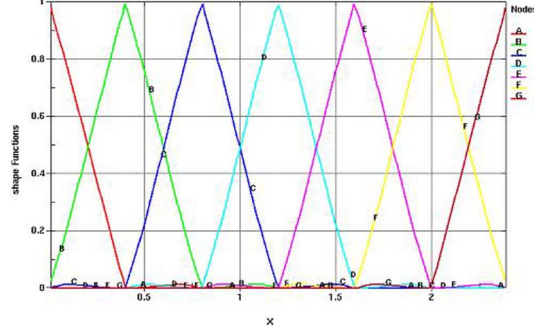
Fig. 2 Convex GMF shape functions with singular kernels

function that is convex and satisfies the Kronecker-delta property. The singular kernel in Fig. 2 is defined as a blending function in Eq. (3) by

$$\Gamma_i(X) = (\tan^{-1}(x - x_i))^{-2} \tag{7}$$

If singularity is applied to all the boundary nodes in multi-dimensional case for the GMF convex approximation, then Eq. (6) becomes

$$\mathbf{conv}(C) = \left\{ \sum_{i=1}^{nb} \Psi_i x_i \middle| x_i \in C, \Psi_i \geq 0, \Psi_i(x_j) = \delta_{ij} \right\} \tag{8}$$

In this paper, we refer the GMF approximation that satisfies Eq. (8) to have a "strong" Kronecker-delta property. The strong Kronecker-delta property is a necessary property for GMF convex approximation to impose the periodic boundary condition in the microscopic analysis of rubber compounds. Other techniques such as the transformation method, Lagrange multiplier and coupling with FEM can be also employed to obtain the strong Kronecker-delta property on the boundary.

2.3. Multi-dimensional GMF approximation

The GMF approximation in multi-dimension is expressed as

$$\Psi_i(\mathbf{x}, \lambda_r) = \frac{\psi_i}{\psi} = \frac{\phi_a(\mathbf{x}; \mathbf{X}_i)\Gamma_i(\mathbf{X}_i, \lambda_r)B(\mathbf{X}_i, \lambda_r, \Theta)}{\Sigma_{j=1}^n \phi_a(\mathbf{x}; \mathbf{X}_j)\Gamma_j(\mathbf{X}_j, \lambda_r)B(\mathbf{X}_i, \lambda_r, \Theta)} \quad \text{for fixed } \mathbf{x} \tag{9}$$

subject to
$$\mathbf{R}_r(\mathbf{x}) = \sum_{i=1}^n \Psi_i \mathbf{X}_i = 0 \quad \text{(linear constraints)} \tag{10}$$

where
$$\psi_i = \phi_a(\mathbf{x}; \mathbf{X}_i)\Gamma_i(\mathbf{X}_i, \lambda_r)B(\mathbf{X}_i, \lambda_r, \Theta) \tag{11}$$

$$\psi = \Sigma_{i=1}^n \psi_1 = \Sigma_{i=1}^n \phi_a(\mathbf{x}; \mathbf{X}_i)\Gamma_i(\mathbf{X}_i, \lambda_r)B(\mathbf{X}_i, \lambda_r, \Theta) \tag{12}$$

$$\mathbf{X}_i = \mathbf{x} - \mathbf{x}_i \tag{13}$$

$\phi_a(\mathbf{x}; \mathbf{X}_i)$ is the weighting function of node i with support size $a(\mathbf{x})$,

$\Gamma_i(\mathbf{X}_i, \lambda_r)$ is the basis function of the GMF approximation,

$\mathbf{x}$ is the coordinate of interior point (fixed point),

$\mathbf{x}_i$ is the coordinate of node i,

n is the number of nodes within the support size $a(\mathbf{x})$ at fixed $\mathbf{x}$,

$\lambda_r(\mathbf{x})(r = 1, 2, \cdots, m)$ are constraint parameters which have to be decided,

m is the number of constraints ($m = 1$ in 1D, $m = 2$ in 2D, and $m = 3$ in 3D),

$B(\mathbf{X}_i, \lambda_r, \Theta)$ is the blending function and Θ is internal functions or variables. The $\lambda_r(\mathbf{x})$ can be obtained by solving

$$\lambda_r(\mathbf{x}) = \arg\left(\mathbf{R}_r(\mathbf{x}) = \sum_{i=1}^{n} \Psi_i\, \mathbf{X}_i = 0 \right) \tag{14}$$

The spatial derivative of the GMF approximation ($B(\mathbf{X}_i, \lambda_r, \Theta) = 1$) is given by

$$\nabla \Psi_i = \Psi_{i,\mathbf{x}} + \Psi_{i,\lambda_r}\lambda_{r,\mathbf{x}} \tag{15}$$

where

$$\Psi_{i,\mathbf{x}} = \frac{\psi_{i,\mathbf{x}}}{\psi} - \Psi_i \sum_{j=1}^{n} \frac{\psi_{j,\mathbf{x}}}{\psi} \tag{16}$$

$$\psi_{i,\mathbf{x}} = \phi_{a,\mathbf{x}}\Gamma_i + \phi_a \Gamma_{i,\mathbf{x}} \tag{17}$$

$$\Psi_{i,\lambda_r} = \frac{\phi_a \Gamma_{i,\lambda_r}}{\psi} - \Psi_i \sum_{j=1}^{n} \frac{\phi_a \Gamma_{j,\lambda_r}}{\psi} \tag{18}$$

$$\lambda_{r,\mathbf{x}} = -\mathbf{J}^{-1}\mathbf{R}_{r,\mathbf{x}} \tag{19}$$

$$\mathbf{J} = \sum_{i=1}^{n} \frac{\phi_a \Gamma_{i,\lambda_r}}{\psi} \otimes \mathbf{X}_i - \mathbf{R}_r \otimes \sum_{j=1}^{n} \frac{\phi_a \Gamma_{j,\lambda_r}}{\psi} \tag{20}$$

$$\mathbf{R}_{r,\mathbf{x}} = \sum_{i=1}^{n} \Psi_{i,\mathbf{x}}\mathbf{X}_i + \delta_{mn} \quad (\delta_{mn}: \text{Kronecker-delta}). \tag{21}$$

By switching the exponential basis function to other functions, the Jacobian matrix ($\mathbf{J}$) is not symmetric in general case.

3. Microscopic analysis of rubber compounds by meshfree method

Multi-scale computational homogenization has received considerable attentions these years due to its ability to provide the macroscopic response of heterogeneous materials with arbitrary microscopic geometry and material behaviors. A first step towards the multi-scale modeling of heterogeneous materials is the modeling of microscopic structure. The microscopic system is modeled by a meshfree method using the unit-cell method based on the concept of a representative volume element (RVE) originally proposed by Hill (1963). The RVE in this study is considered to consist of a soft matrix and reinforced particles as illustrated in Fig. 3. The reinforced particles can be aggregated and randomly distributed in RVE. The RVE should be large enough to contain sufficient information about the microstructure in order to be representative, at the same time it
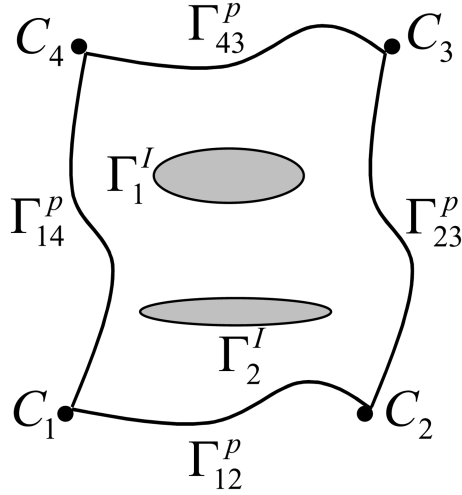
Fig. 3 Two-dimensional unit cell

should be small enough to represent the microstructure. In addition, all statistical information about the material is supposed to be available in one single realization of representative volume, which is known as the ergodicity assumption (Van der Sluis *et al.* 2001). The RVE is regarded as a heterogeneous material with spatially varying, but known constitutive properties (Nemat-Nasser and Hori 1993). The micro-macro relationship of the rubber compound is then determined by estimating the relevant stress-strain constitutive from the RVE to the associated macroscopic point (Gauss point) using various multi-scale computational homogenization methods.

3.1. Microscopic boundary conditions

Different types of boundary conditions can be applied to the unit cell. In this paper, we consider the periodic boundary conditions. This choice has been justified by many authors (Terada *et al.* 2000, Van der Sluis *et al.* 2001) to show that periodicity conditions render a more reasonable estimation of the stress-strain constitutive than uniform displacement and uniform traction boundary conditions. The periodic boundary condition in a two-dimensional plane strain unit cell is given by (Smit *et al.* 1998)

$$u\big|_{\Gamma^p_{43}} = u\big|_{\Gamma^p_{12}} - u\big|_{C1} + u\big|_{C4} \tag{22}$$

$$u\big|_{\Gamma^p_{14}} = u\big|_{\Gamma^p_{23}} - u\big|_{C2} + u\big|_{C1} \tag{23}$$

where Γ^p_{ij} is the edge of unit cell subject to periodic condition in Fig. 3 and Ci is the vertices in the unit cell. $u\big|_{Ci}$ denotes the position vector of vertices Ci with respect to some fixed reference system.

The periodic boundary conditions imply that the deformation of each boundary pair is equal and the stress vector are opposite in sign on each pair. In order to prevent the rigid body rotation in the unit cell, an extra constraint is added as follows:

$$u\big|_{C3} = u\big|_{C4} - u\big|_{C1} + u\big|_{C2} \tag{24}$$

It is recognized that the weak Kronecker-delta property from Eq. (6) is readily applied to the interfaces $\Gamma^I = \Gamma_1^I + \Gamma_2^I$ between matrix and inclusions if both matrix and inclusions are modeled by convex GMF approximations. The weak Kronecker-delta property on the interface guarantees the continuity of displacement across the interface. In contrast, a "strong" Kronecker-delta property is required for each node along the interface if inclusion is not modeled by the convex GMF approximation such as FEM approximation or non-convex GMF approximation. The strong Kronecker-delta property is also required on the periodic boundary $\Gamma^p = \Gamma_{12}^p + \Gamma_{23}^p + \Gamma_{43}^p + \Gamma_{14}^p$ or on the interface if the de-bonding is considered in the analysis. The strong Kronecker-delta property is gained by the introduction of singularity for all the boundary nodes along periodic boundary Γ^p and de-bonding interface with Eq. (7).

3.2. Periodic boundary conditions via multiple constrains

Eqs. (22-24) can be considered as the dependent multiple constraint equations. In order to solve the multiple constraint equations using the convex GMF approximation for arbitrary loading conditions, we have adopted the transformation method (Cook et al. 1998). Alternatives such as the Lagrange multipliers and penalty method can also be considered. Eqs. (22-24) can be rearranged and written in matrix form as

$$\Phi_n^K(U) = 0 \ \text{ or } \ [C]\{U_p\} = \{0\} \tag{25}$$

where $[C]$ is the matrix contains the coefficients of the constraint equations and $\{U_p\}$ is the corresponding periodic d.o.f.s.. Gaussian elimination can be applied to the $[C]$ matrix on the left of Eq. (25) such that Eq. (25) can be further partitioned as

$$[C_e \ C_c]\begin{Bmatrix} U_e \\ U_c \end{Bmatrix} = \{0\} \tag{26}$$

where $\{U_c\}$ is the displacement vector with a collection of independent nodes and $\{U_e\}$ is the displacement vector contains the nodes that need to be eliminated. $[C_e \ C_c]$ is the corresponding coefficient matrix, where matrix $[C_e]$ is square and non-singular. We can express $\{U_e\}$ using Eq. (26) in the following form

$$\{U_e\} = -[C_e]^{-1}[C_c]\{U_c\} = [L]\{U_e\} \tag{27}$$

where

$$[L] = -[C_e]^{-1}[C_c] \tag{28}$$

Matrix $[L]$ describes the relationship of dependent nodes $\{U_e\}$ and independent nodes $\{U_c\}$.

Consequently, the constraint equations associated with the periodic boundary conditions can be written as

$$\{U_p\} = \begin{Bmatrix} U_e \\ U_c \end{Bmatrix} = [\bar{T}]\{U_c\} \tag{29}$$

where $[\bar{T}]$ is the local transformation matrix involves the periodic boundary conditions and is defined as

$$[\bar{T}] = \begin{bmatrix} L \\ I \end{bmatrix} \qquad (30)$$

and I denotes the unit tensor.

The global displacements now becomes

$$\{U\} = \begin{Bmatrix} U_e \\ U_c \\ U_i \end{Bmatrix} = [\tilde{T}]\{U_r\} \qquad (31)$$

with

$$\{U_r\} = \begin{Bmatrix} U_c \\ U_i \end{Bmatrix} \qquad (32)$$

and

$$[\tilde{T}] = \begin{bmatrix} \bar{T} & 0 \\ 0 & I \end{bmatrix} \qquad (33)$$

where $\{U_r\}$ is the retained nodes that includes the independent nodes $\{U_c\}$ in the constraint equations and the rest of nodes $\{U_i\}$ in the unit cell that do not involve the constraint equations. $[\tilde{T}]$ is the global transformation matrix that contains the local transformation matrix in Eq. (30) and an unit tensor. The global transformation matrix carries the information of retained nodes and eliminated nodes that can be used to condense the structural equations for the solving of periodic boundary value problem. This is described in the following section.

4. Meshfree Galerkin formulations with periodic boundary conditions

4.1. Nonlinear meshfree formulation with convex GMF approximation

The weak form for the momentum equation of a non-linear elasticity problem is expressed by

$$\delta\Pi(\boldsymbol{u}) = \delta W^{kin} + \delta W^{int} - \delta W^{ext} \qquad (34)$$

where δW^{kin} is the virtual kinetic work from inertia, δW^{int} is the virtual internal work and δW^{ext} is the virtual external work. In total Lagrangian format, it is defined in the initial configuration by

$$\delta\Pi(\boldsymbol{u}) = \int_{\Omega_0} \delta u_i \rho_0 \ddot{u}_i d\Omega + \int_{\Omega_0} \delta E_{ij} \frac{\partial W(\boldsymbol{u})}{\partial E_{ij}} d\Omega - \delta W^{ext}(\boldsymbol{u})$$

$$= \int_{\Omega_0} \delta u_i \rho_0 \ddot{u}_i d\Omega + \int_{\Omega_0} \delta E_{ij} S_{ij}(\boldsymbol{u}) d\Omega - \delta W^{ext}(\boldsymbol{u}) = 0 \qquad (35)$$

where $S_{ij} = \dfrac{\partial W}{\partial E_{ij}}$ is the second Piola-Kirchhoff stress, W is the strain energy density function and E_{ij}

is the Green-Lagrangian strain. In quasi-static analysis, the acceleration in Eq. (35) is dropped. The linearization of Eq. (35) leads to the iterative equation in quasi-static analysis given by

$$\Delta \delta \Pi(\boldsymbol{u}) = \int_{\Omega_0} \delta E_{ij} \frac{\partial W(\boldsymbol{u})}{\partial E_{ij} \partial E_{kl}} \Delta E_{kl} d\Omega - \delta W^{ext}(\boldsymbol{u})$$

$$= \int_{\Omega_0} \delta E_{ij} [D_{ijkl} + T_{ijkl}] \Delta E_{kl} d\Omega - \delta W^{ext}(\boldsymbol{u}) \tag{36}$$

where $D_{ijkl} = \dfrac{\partial^2 W}{\partial E_{ij} \partial E_{kl}}$ and $T_{ijkl} = \delta_{ik} S_{jl}$. Using the discrete GMF approximation, the discrete iterative equation of Eq. (36) is obtained as

$$\delta [\boldsymbol{U}]^T \boldsymbol{K}_{n+1}^v (\Delta [\boldsymbol{U}])_{n+1}^{v+1} = -\delta [\boldsymbol{U}]^T \boldsymbol{F}_{n+1}^v \tag{37}$$

where tangent stiffness matrix $\boldsymbol{K}_{n+1}^v (\Delta [\boldsymbol{U}])_{n+1}^{v+1}$ contains the material and geometric stiffness matrices that evaluated at the vth iteration during the $(n+1)$ time incremental step. $\boldsymbol{K}_{n+1}^v$ is the residual nodal force vector.

By taking the variation of Eq. (31) and substituting into Eq. (37), one can obtain the reduced discrete equations by

$$\delta \{\boldsymbol{U}_r\}^T [\tilde{\boldsymbol{T}}]^T \boldsymbol{K}_{n+1}^v [\tilde{\boldsymbol{T}}] (\Delta \{\boldsymbol{U}_r\})_{n+1}^{v+1} = -\delta \{\boldsymbol{U}_r\}^T [\tilde{\boldsymbol{T}}]^T \boldsymbol{F}_{n+1}^v \tag{38}$$

which is used to solve the periodic boundary value problem in quasi-static analysis and to obtain the displacement vector $\{\boldsymbol{U}_r\}$ of the retained nodes.

Finally, the displacements of dependent nodes $\{\boldsymbol{U}_e\}$ are obtained using Eq. (27).

For explicit time integration, we perform a row-sum method to construct a lump mass in Eq. (35) (Chen *et al.* 1996). The corresponding discrete equation in explicit analysis is

$$[\tilde{\boldsymbol{M}}_r]\{\ddot{\boldsymbol{U}}_r\} = \{\tilde{\boldsymbol{F}}_r\} \tag{39}$$

with

$$[\tilde{\boldsymbol{M}}_r] = [\tilde{\boldsymbol{T}}]^T [\boldsymbol{M}^{row-sum}][\tilde{\boldsymbol{T}}] \tag{40}$$

where $[\tilde{\boldsymbol{M}}_r]$ is the mass matrix of retained nodes in diagonal form which is obtained form the transformed row-sum mass matrix $[\boldsymbol{M}^{row-sum}]$ using the global transformation matrix. Eq. (40) needs to be computed only once in the explicit analysis. The final form of discrete equations in the explicit analysis becomes

$$\{\ddot{\boldsymbol{U}}_r\} = [\tilde{\boldsymbol{M}}_r]^{-1} [\tilde{\boldsymbol{T}}^T]\{\boldsymbol{F}\} \tag{41}$$

Consequently, the accelerations, velocities and displacements of the eliminated nodes can be obtained using Eq. (27).

4.2. Interface de-bonding with explicit analysis

In this section, we incorporate the cohesive zone model into the meshfree analysis of interface de-bonding in the rubber compound. Within the meshfree Galerkin framework, the discretization of the interface de-bonding representation is accomplished by the introduction of interface elements along
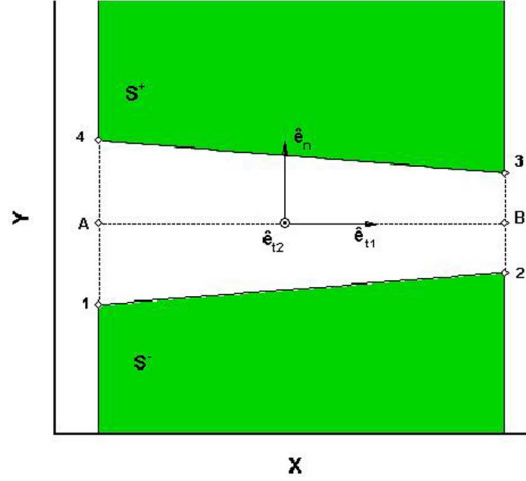
Fig. 4 Interface element in deformed configuration

the interfaces between the rubber matrix and reinforced particles. Apparently, this requires a strong Kronecker-delta property of GMF approximation for the boundary nodes along the material interface. For this purpose, the singular kernel method is adopted in the construction of convex GMF approximation for the meshfree de-bonging analysis.

Fig. 4 shows an interface element in deformed configuration with the normal vector of interface points into the S^+ side of interface. Subsequently, the tangent vector can be defined as follows:

$$\hat{e}_{t1} = \left(\frac{\partial x}{\partial \xi}, \frac{\partial y}{\partial \xi} \right) \bigg/ \left\| \left(\frac{\partial x}{\partial \xi}, \frac{\partial y}{\partial \xi} \right) \right\| \tag{42}$$

The natural coordinates ($\hat{e}_n$, $\hat{e}_{t1}$) define a local coordinate system in the deformed configuration of the element. At time $=0.0$, Points 1 and 4 coincide with point A and points 2 and 3 coincide with point B. According, the position vector $\overline{AB}$ in Fig. 4 represents the mid-plane of the element. After de-bonding, the displacement vectors of points $\mathbf{X}^A$ and $\mathbf{X}^B$ can be expressed in terms of displacements at point 1 to 4 by

$$\begin{Bmatrix} u_x^A \\ u_y^A \\ u_x^B \\ u_y^B \end{Bmatrix} = [\boldsymbol{H}]\{\boldsymbol{u}_a\} = \begin{bmatrix} -1 & 0 & 0 & 0 & 0 & 0 & 1 & 0 \\ 0 & -1 & 0 & 0 & 0 & 0 & 0 & 1 \\ 0 & 0 & -1 & 0 & 1 & 0 & 0 & 0 \\ 0 & 0 & 0 & -1 & 0 & 1 & 0 & 0 \end{bmatrix} \begin{Bmatrix} u_x^1 \\ u_y^1 \\ u_x^2 \\ u_y^2 \\ u_x^3 \\ u_y^3 \\ u_x^4 \\ u_y^4 \end{Bmatrix} \tag{43}$$

The relative displacements of interface element defined in the local coordinate system can be obtained using the FEM shape functions as

$$
\begin{Bmatrix} u_x \\ u_y \end{Bmatrix}_{\xi_1} = [\boldsymbol{N}^l]\{\bar{u}\} = \begin{bmatrix} N_1^l & 0 & N_2^l & 0 \\ 0 & N_1^l & 0 & N_2^l \end{bmatrix} \begin{Bmatrix} u_x^A \\ u_y^A \\ u_x^B \\ u_y^B \end{Bmatrix} \tag{44}
$$

The relative displacement vector in Eq. (44) is also called the "displacement jumps" or "opening displacements" over the cohesive surface (Ortiz and Pandolfi 1999) in the cohesive zone model.

By substituting Eq. (44) into Eq. (43), one can obtain the displacement jumps as

$$
\begin{Bmatrix} u_t \\ u_n \end{Bmatrix}_{\xi_i} = [T_g]^T[\boldsymbol{N}^l][\boldsymbol{H}]\{\boldsymbol{u}_a\} \tag{45}
$$

where

$$
[T_g] = [\{\hat{\boldsymbol{e}}_n\}, \{\hat{\boldsymbol{e}}_t\}] = \begin{bmatrix} e_n^x & e_{t1}^x \\ e_n^y & e_{t1}^y \end{bmatrix} \tag{46}
$$

Obviously, the displacement jumps remain invariant upon superposed rigid translations of the interface element. The cohesive tractions are obtained using a bi-linear cohesive law (Zavattieri and Espinosa 2001) defined by the following expressions

$$
T_n = \frac{27}{4} T_{\max}\left(\frac{u_n}{\delta_n}\right)(1 - 2\lambda_{cr} + \lambda_{cr}^2)\frac{\lambda}{\lambda_{cr}}
$$

$$
T_t = \frac{27}{4} \alpha T_{\max}\left(\frac{u_t}{\delta_t}\right)(1 - 2\lambda_{cr} + \lambda_{cr}^2)\frac{\lambda}{\lambda_{cr}}
$$

$$
\lambda = \sqrt{\left(\frac{u_n}{\delta_n}\right)^2 + \left(\frac{u_t}{\delta_t}\right)^2} \tag{47}
$$

where T_n is the normal traction, T_t is the tangential traction and T_{max} is the maximum normal traction that the interface can bear before failure. Noted that the cohesive tractions are defined on an un-deformed area per uint. The material constants involved in Eq. (47) include: δ_n and δ_n are critical values at which de-bonding takes place in normal and tangential directions respectively, α is the parameter coupling normal and shear tractions and λ_{cr} is the critical displacement jump.

Accordingly, the nodal forces follow from the tractions are obtained by

$$
\{\boldsymbol{F}\} = [T_g]\{\boldsymbol{F}\} \tag{48}
$$

where

$$
\{\boldsymbol{F}'\} = \int_{l'} [\boldsymbol{N}^l]^T[\boldsymbol{T}]dl' \tag{49}
$$

(a) Loading case I   (b) Loading case II
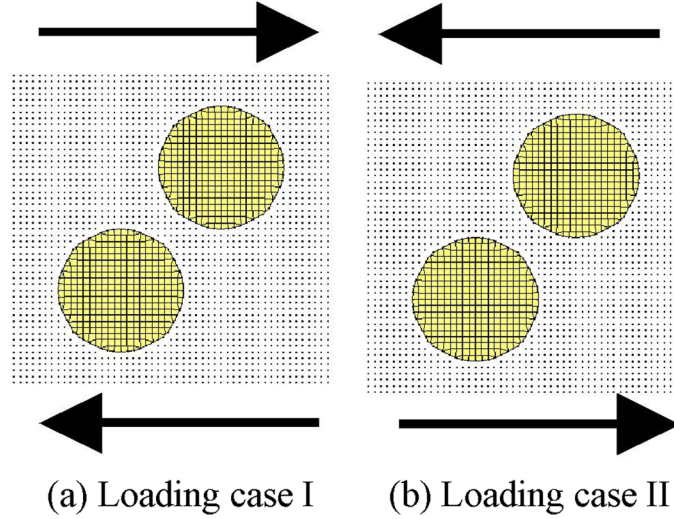
Fig. 5. Two loading cases in shear test

Finally, the Eq. (49) is added into the right hand side of Eq. (41) for the microstructures de-bonding analysis under periodic boundary condition.

5. Numerical examples

5.1 Shear test of regular rubber filler

In this example, a plane strain shear test is simulated on a unit cell with two regular fillers. Two loading cases as shown in Fig. 5(a) and (b) are analyzed to study the shear response of anisotropic rubber compounds under periodic boundary conditions. The rubber matrix is modeled by Yeoh's cubic strain energy density function in Eq. (50) with coefficients $C_{10} = 0.333$ MPa, $C_{20} = 0.0$ MPa, $C_{30} = 5.05E\text{-}04$ MPa and bulk modulus $k = 333.0$ MPa. The density of rubber matrix is 0.945 g/cm^3. The filler is modeled by a linear elastic material with high Young's modulus $E = 1.0E + 04$ MPa, and Poisson's ratio $v = 0.3$. The filler density is 10.08 g/cm^3. The dimension of unit cell is 5 cm × 5 cm and the radius of the filler is 1 cm such that the volume fraction is about 25.1%. Expontional basis function is chosen as the basis function in GMF approximation. Normalized support size = 1.5 is used together with 2 × 2 × 2 Gaussian quadrature in the meshfree computation.

$$W(I_1) = C_{10}(I_1 - 3) + C_{20}(I_1 - 3)^2 + C_{30}(I_1 - 3)^3 \qquad (50)$$

The loading case I is first analyzed using both implicit (quasi-static) and explicit analysis. The comparison of shear load history with implicit and explicit analysis is presented in Fig. 6(a) and with the zoom-in plot in Fig. 6(b). The predicted shear load using explicit analysis is almost identical to the solution predicted by the implicit analysis except small oscillation is observed in the explicit analysis. The oscillation is only observed in the early loading stage and does not appear in the large deformation range. The oscillation is probably due to the nature of explicit analysis in the

(a) Full scale plot   (b) Zoon-in plot
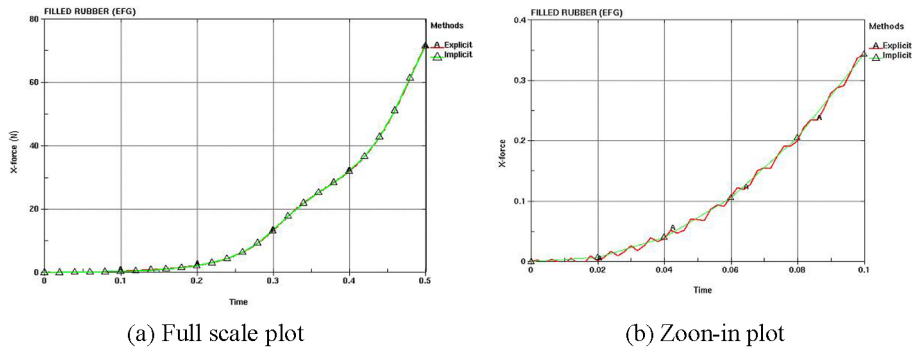
Fig. 6. Comparison of shear load history curves with explicit and implicit analysis
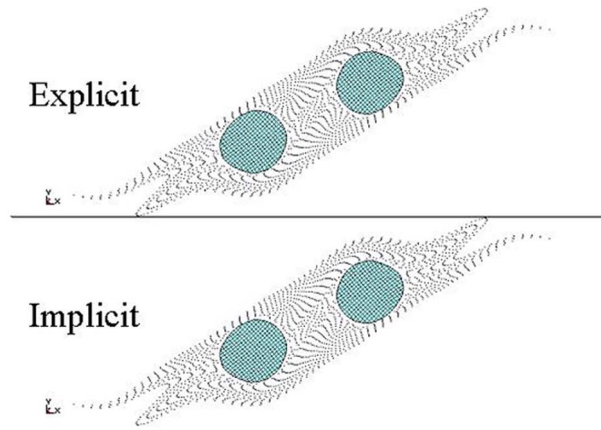
Fig. 7 Comparison of final deformation at 200% shear strain

Table 1. CPU time comparison of explict and implict analysis in shear test

	Explicit	Implicit
Norm. CPU	117.0	1.0

rubber-like material when loading speed is high. Fig. 7 shows the comparison of final deformation at 200% shear strain using implicit and explicit methods in loading case I. The final deformation in explicit and implicit analysis agrees well with each other. A comparison of normalized CPU time using implicit and explicit methods is listed in Table 1.

In the loading case II, only the implicit analysis is conducted. To study the influence of rubber filler in the shear response of the rubber compounds, a shear test is also simulated on the unit cell without the consideration of rubber filler. The comparison of resulting stress-strain curves in loading case I, II and the case without rubber filler is given in Fig. 8. Apparently, rubber filler plays a role in the stiffing of rubber compounds. For case I and II, the orientation of rubber filler determines the anisotropy of shear responses. Fig. 9 compares the final deformation of case I and case II measured at 200% shear strain.
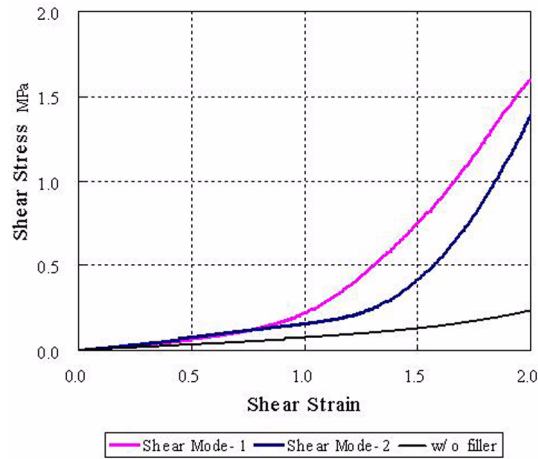
Fig. 8 Comparison of shear stress-strain curves in three cases
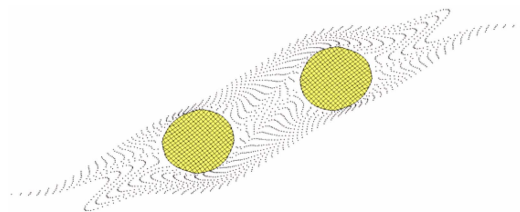
(a) Final deformation in loading case I
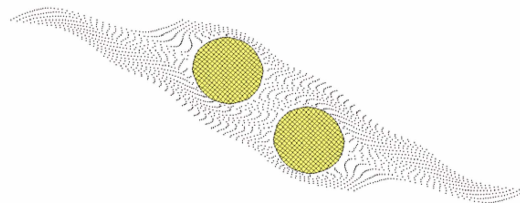
(b) Final deformation in loading case II

Fig. 9 Comparison of final deformation in loading case I and II

5.2 Tensile test of irregular rubber filler

This example studies the influence of morphology of fillers in the micro-mechanical behavior of rubber compounds. Two filler morphologies in the unit cell shown in Fig. 10 are tested in this example. The plane strain unit cell is subjected to a macroscopic tensile loading with same material parameters and same unit cell size used in example 5.1. The volume fraction of filler is about 46% in two models. The quasi-static analysis is adopted in this example. Same numerical parameters such as normalized support and integration order are also the same as these used in example 5.1.

Fig. 11 shows the nominal stress-strain curves resulted from the model A and model B. It is

(a) model A   (b) model B
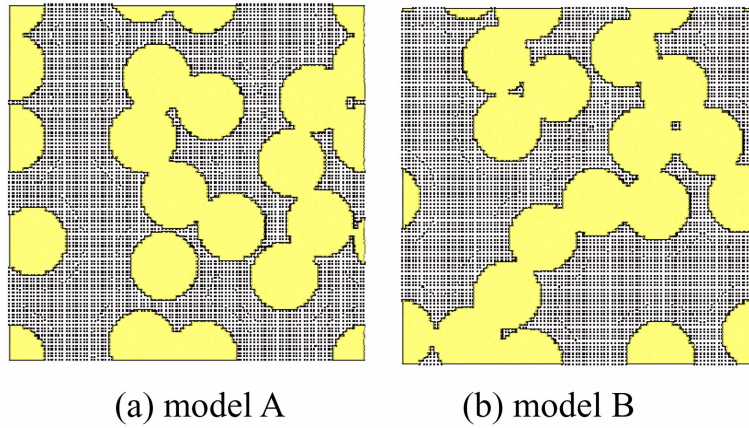
Fig. 10 Two irregular rubber filler models in the tensile test
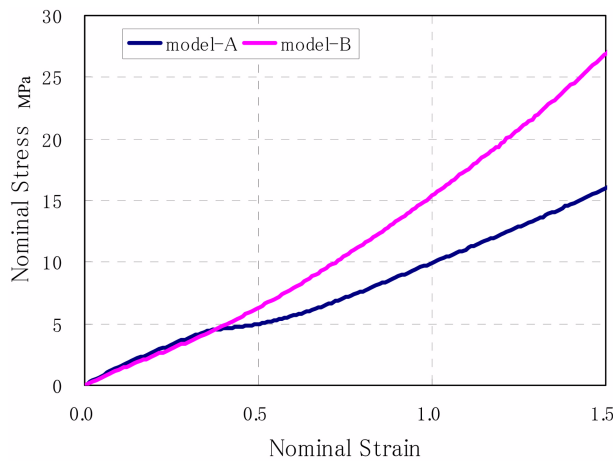
Fig. 11 Comparison of nominal stress-strain curves by two models

observed the aggregated filler of model B exhibits a stiffer response than the averaged random filer of model A in the large deformation range. This is confirmed by their deformed plots at 100% macroscopic strain shown in Fig. 12. In Fig. 12, the aggregated filler of model B displays a highly localized deformation than the averaged random filer of model A. Those high deformation results in a stiff material response in model B. It can thus be concluded that, as the fillers become more aggregated and irregularly distributed in the matrix, the overall mechanical response of rubber compounds behaves more stiff.

5.3 De-bonding analysis of rubber compounds

This example focuses on the analysis of interfaces de-bonding between the matrix and the inclusion under periodic boundary condition. A unit cell consisted of stiff inclusions in an elastic matrix material is subjected to a bi-axial loading as shown in Fig. 13. The dimension of the unit cell is 3 cm × 3 cm and the loading speed is 0.1 cm/s in x-direction and 0.04 cm/s in y-direction. The
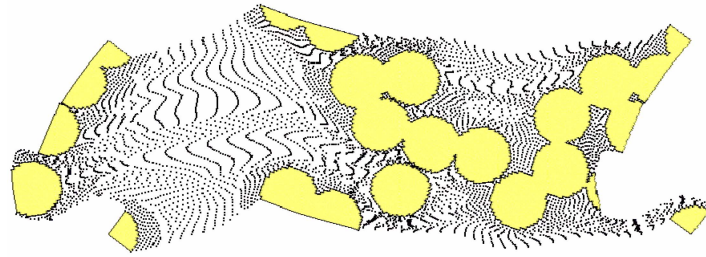
(a) Model A
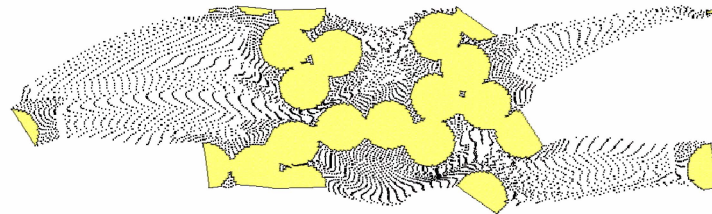
(b) Model B

Fig. 12 Deformation at 100% macroscopic strain
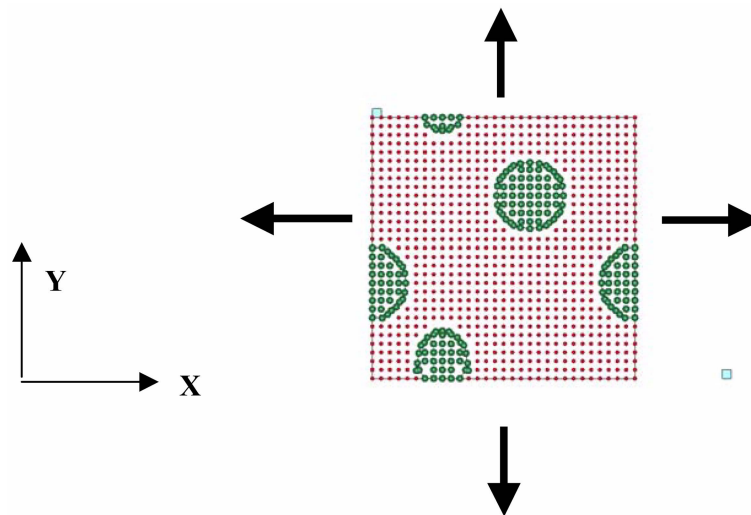
Fig. 13 A de-cohesive rubber compound subjected to a bi-axial tensile loading

analysis is conducted by the explicit time integration method. The degrading interface between the matrix and the inclusion is modeled by means of a bi-linear cohesive model defined in Equation (47). The cohesive parameters used in the cohesive model are: $T_{max} = 50$ MPa, $\delta_n = \delta_t = 0.1$ cm, $\alpha = 0.5$ and $\lambda_{cr} = 1.0$.

(a) Elastic matrix   (b) Mooney-Rivlin rubber matrix
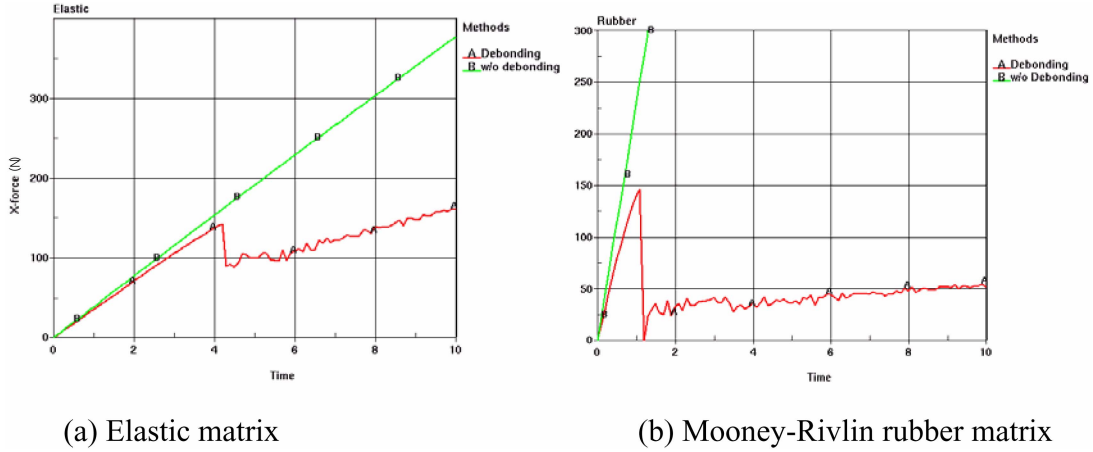
Fig. 14 The de-bonding analysis in two matrix materials

Two elastic matrix materials are considered in this example. The first rubber matrix is modeled by Mooney-Rivlin model. The strain energy density function of Mooney-Rivlin model is described in Eq. (51) with material constants $C_{10} = 6.0$ MPa, $C_{01} = 1.0$ MPa, and bulk modulus $k = 1395.0$ MPa in this example. The density in first rubber matrix is 1.15 g/cm^3. The second matrix material is modeled by a linear elastic material with Young's modulus $E = 2.1E + 02$ MPa and Poisson's ratio $v = 0.3$. The density of second rubber is 1.52 g/cm^3. The filler is modeled by a linear elastic material with a relatively high Young's modulus $E = 2.1E + 03$ MPa, Poisson's ratio $v = 0.3$ and density equals to 10.00 g/cm^3. Same numerical parameters in meshfree method such as normalized support and integration order are the same as these used in example 5.1.

$$W(I_1, I_2) = C_{10}(I_1 - 3) + C_{01}(I_2 - 1) \tag{51}$$

The force comparison of de-bonding and non-de-bonding models with elastic matrix is presented in Fig. 14(a) and with Mooney-Rivlin matrix presented in Fig. 14(b) respectively. Different initial slopes of force curves are observed in the de-bonding and non-de-bonding models indicate the use of initially-elastic cohesive model in the de-bonding analysis. The use of the initially-elastic cohesive model in the interfaces can be considered as the insertion of an elastic bonding material between matrix and inclusions. Both elastic matrix and Mooney-Rivlin rubber matrix materials show a sudden drop of force curve representing the onset of the failure in the bonding interfaces. It is remarked that, because of the usage of same cohesive parameters in the de-bonding analysis, the predicated peak force in elastic matrix is almost the same as that in Mooney-Rivlin rubber matrix. It is also observed that the force magnitude in the post-failure range is gradually picking up as the deformation increases. The force magnitude in the post-failure range is determined by the strength of matrix material. This can be confirmed by the progressive deformation of elastic and Mooney-Rivlin rubber models shown in Fig. 15 (a) and (b). Finally, Fig. 16 shows the arrangement of unit cell in large deformation with respect to its neighboring RVEs to demonstrate a good agreement of periodic boundary condition.

It is noted that the conventional first-order computational homogenization methods may not be applied to this problem, since thy leads to an ill-posed problem on the macroscale level. To
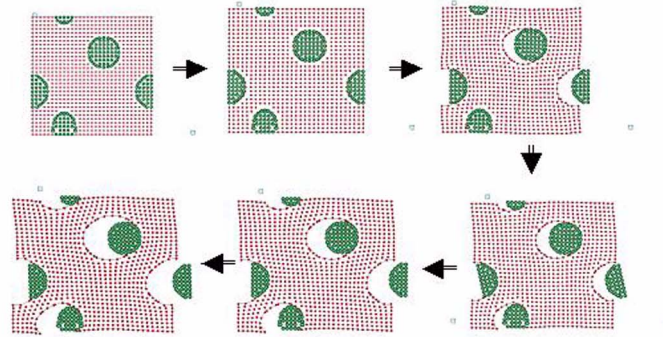
(a) Progress deformation of rubber compound with elastic matrix
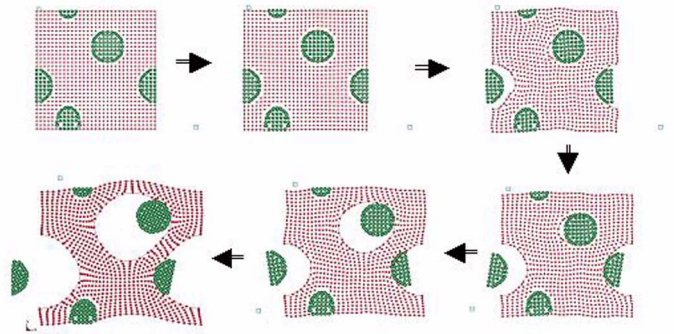
(b) Progress deformation of rubber compound with Mooney-Rivlin rubber matrix

Fig. 15 Progress deformation in two matrix materials
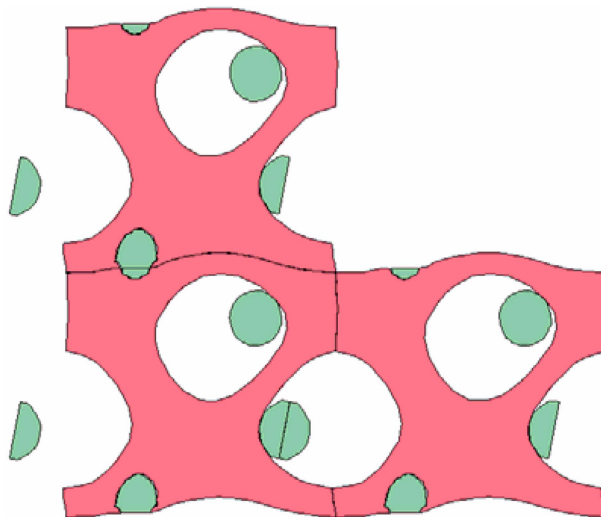
Fig. 16. Check of periodicity

overcome this difficulty, a second-order computational homogenization methods or multi-scale aggregating discontinuities method (Belytschko *et al.* 2008) can be considered.

6. Conclusions

In this paper, we present a meshfree procedure using a convex generalized meshfree (GMF) approximation for the large deformation analysis of particle-reinforced rubber compounds on microscopic level. The convex GMF approximation is generated by choosing the positive and monotonic increasing basis function. The convex GMF approximation poses the weak Kronecker-delta property on the boundary such that the continuity of displacement across the material interface in the rubber compounds is guaranteed. In order to impose the periodic boundary condition in the unit cell method for the microscopic analysis, a singular kernel is incorporated with the GMF basis function on the periodic boundary nodes to acquire the desired strong Kronecker-delta property on the periodic boundary. As a result, the imposition of boundary conditions in the meshfree analysis is simplified and the smoothness of the meshfree approximation is kept.

To solve the periodic boundary condition numerically, a transformation method based on the multiple constraints concept is employed. The computational formulation is formed in the framework of Galerkin meshfree method based on a generalized meshfree approximation. The final discrete equations are condensed and solved for the retained nodes. The dependent nodes are obtained from the constraint equations. Both implicit and explicit formations are presented. In order to consider the de-bonding phenomena in the microscopic analysis of rubber compound, the cohesive interface element formation is also derived in conjunction with explicit meshfree formulation.

The presented meshfree procedure provides an effective way to perform the microscopic analysis of rubber compounds involving large deformation and interface de-bonding. Several benchmarks have been investigated to demonstrate the effectiveness of this approach. They include the study of shear loading effect, the influence of filler morphology and the de-bonding in different rubber matrices. This enables the straightforward application of the method to the micro-macro modeling of heterogeneous materials in large deformation using various homogenization methods and will be presented in our other papers in the near future.

Acknowledgements

References

Arroyo, M. and Ortiz, M. (2006), "Local maximum-entropy approximation schemes: a seamless bridge between finite elements and meshfree methods", *Int. J. Numer. Meth. Eng.*, **65**, 2167-2202.
Belikov, V. V. and Semenov, A. Y. (2000), "Non-Sibsonian interpolation on arbitrary system of points in Euclidean space and adaptive isolines generation", *Appl. Number. Math.*, **32**(4), 371-387.
Belytschko, T., Lu, Y. Y., and Gu, L. (1994), "Element-free Galerkin methods", *Int. J. Numer. Meth. Eng.*, **37**(2),

229-256.

Belytschko, T., Organ, D. and Krongauz, Y. (1995), "A coupled finite element-element-free Galerkin method", *Comput. Mech.*, **17**, 186-195.

Belytschko, T., Krongauz, Y., Organ, D., Fleming, M. and Krysl, P. (1996), "Meshless methods: An overview and recent developments", *Comput. Meth. Appl. Mech. Eng.*, **139**, 3-47.

Belytschko, T., Loehnert, S. and Song, J. H. (2008), "Multiscale aggregating discontinuities: A method for circumventing loss of material stability", *Int. J. Numer. Meth. Eng.*, **73**, 869-894.

Chen, J. S., Pan, C., Wu, C. T. and Liu, W. K. (1996), "Reproducing kernel particle methods for large deformation analysis of non-linear structures", *Comput. Meth. Appl. Mech. Eng.*, **139**, 195-227.

Chen, J. S. and Wang, H. P. (2000), "New boundary condition treatments in meshfree computation of contact problems", *Comput. Meth. Appl. Mech. Eng.*, **187**, 441-468.

Chen, J. S. and Mehraeen, S. (2004), "Variationally consistent multi-scale modeling and homogenization of stressed grain growth", *Comput. Meth. Appl. Mech. Eng.*, **193**, 1825-1848.

Chen, J. S. and Mehraeen, S. (2005), "Multi-scale modeling of heterogeneous materials with fixed and evolving microstructures", *Model. Simul. Mater. Sc.*, **13**, 95-121.

Chen, J. S., Hu, W. and Hu, H. Y. (2008), "Reproducing kernel enhanced local radial basis collocation method", *Int. J. Numer. Meth. Eng.*, **75**, 600-627.

Cook, R. D., Malkus, D. S. and Plesha, M. E. (1998) Concepts and Applications of Finite Element Analysis, John Wiley & Sons, New York.

Duchon, J. (1977), "Splines minimizing rotation-invariant semi-norms in Sobolev spaces", in Constructive Theory of Functions of Several Variables, Oberwolfach 1976, W. Schempp and K. Zeller (eds.), Springer Lecture Notes in Math. 571, Springer-Verlag, Berlin, 85-100.

Gu, L. (2003), "Moving kriging interpolation and element-free Galerkin method", *Int. J. Numer. Meth. Eng.*, **56**, 1-11.

Hill, R. (1963), "Elastic properties of reinforced solids: some theoretical principles", *J. Mech. Phys Solid*, **11**, 357-372.

Hu, H. Y., Chen, J. S. and Hu, W. (2007), "Weighted radial basis collocation method for boundary value problems", *Int. J. Numer. Meth. Eng.*, **69**, 2736-2757.

Jaynes, E. T. (1957), "Information theory and statistical mechanics", *Physical Review*, **106**(4), 620-630.

Kansa, E. J. (1992a), 'Multiqudrics - a scattered data approximation scheme with applications to computational fluid dynamics - I. Surface approximations and partial derivatives", *Comput. Math. Appl.*, **19**, 127-145.

Kansa, E. J. (1992b), "Multiqudrics - a scattered data approximation scheme with applications to computational fluid dynamics - II. Solutions to parabolic, hyperbolic and elliptic partial differential equations", *Comput. Math. Appl.*, **19**, 147-161.

Lancaster, P. and Salkauskas, K. (1981), "Surfaces generated by moving least squares methods", *Math. Comput.*, **37**, 141-158.

Li, S. and Liu, W. K. (2002), "Meshfree and particle methods and their applications", *Appl. Mech. Review.*, **55**, 1-34.

Liu, G. R. and Gu, Y. T. (2001), "A point interpolation method for two-dimensional solids", *Int. J. Numer. Meth. Eng.*, **50**, 937-951.

Liu, W. K., Jun, S. and Zhang, Y. F. (1995), "Reproducing kernel particle methods", *Int. J. Numer. Meth. Fluids.*, **20**, 1081-1106.

Lucy, L. (1977), "A numerical approach to testing the fission hypothesis", *Astron. J.*, **82**, 1013-1024.

Nemat-Nasser, S., Hori, M. (1993), Micromechanics: Overall Properties of Heterogeneous Materials, Elsevier, Amsterdam.

Ortiz, M. and Pandolfi, A. (1999), "Finite-deformation irreversible cohesive elements for three-dimensional crack-propagation analysis", *Int. J. Numer. Meth. Fluids.*, **44**, 1267-1282.

Powell, M. J. D. (1992), "The theory of radial basis function approximation in 1990", in Advances in Numerical Analysis, Light FW (edn), Oxford University Press, Oxford, 303-322.

Rabczuk, T., Xiao, S. P. and Sauer, M. (2006), "Coupling of mesh-free methods with finite elements: basic concepts and test results, *Commun. Numer. Meth. Eng.*, **22**, 1031-1065.

Shannon, C. E. (1948), "A mathematical theory of communication", *Bell Syst. Tech. J.*, **27**, 379-423.

Smit, R. J. M, Brekelmans, W. A. M. and Meijer, H. E. H. (1998), "Prediction of the mechanical behavior of nonlinear heterogeneous systems by multi-level finite element modeling", *Comput. Meth. Appl. Mech. Eng.*, **155**, 181-192.

Sukumar, N. (2004), "Construction of polygonal interpolants: a maximum entropy approach", *Int. J. Numer. Meth. Eng.*, **61**, 2159-2181.

Terada, K, Hori, M., Kyoya, T. and Kikuchi, N. (2000), "Simulation of the multi-scale convergence in computational homogenization approaches", *Int. J. Solids Struct.*, **37**, 2285-2311.

Terada, K., Asai, M. and Yamagishi, M. (2003), "Finite cover method for linear and nonlinear analysis of heterogeneous solids", *Int. J. Numer. Meth. Eng.*, **58**, 1321-1346.

Van der Sluis, O., Schreurs, P. J. G. and Meijer, H. E. H. (2001), "Homogenization of structured elastoviscoplastic solids at finite strains", *Mech. Mater.*, **33**, 499-522.

Wang, D, Chen, J. S. and Sun, L. (2003), "Homogenization of magnetostrictive particle-filled elastomers using an interface-enriched reproducing kernel particle method", *Finite Elem. Anal. Design.*, **39**, 765-782.

Wu, C. T., Park, C. K. and Chen, J. S. (2009), "A generalized meshfree approximation for the meshfree analysis of solid", *Int. J. Numer. Meth. Eng.*, submitted.

Zavattieri, P. D. and Espinosa, H. D. (2001), "Grain level analysis of ceramic microstructures subjected to normal impact loading", *Acta Materialia*, **49**(20), 4291-4311.